

Geophysical Research Letters®
















RESEARCH LETTER

10.1029/2023GL103069

The First Ground Level Enhancement Seen on Three Planetary Surfaces: Earth, Moon, and Mars

Key Points:

- This is the first ground level enhancement event simultaneously measured on Earth, Moon, and Mars
- We analyze the radiation measurements at 3 locations and compare with our model predictions based on detected solar energetic particle (SEP) flux
- We show that extreme SEP events can induce much higher (~100 times) radiation doses on the Moon than on Mars

Jingnan Guo^{1,2} , Xiaolei Li¹ , Jian Zhang¹ , Mikhail I. Dobynde¹ , Yuming Wang^{1,2} , Zigong Xu³ , Thomas Berger⁴ , Jordanka Semkova⁵ , Robert F. Wimmer-Schweingruber³ , Donald M. Hassler⁶ , Cary Zeitlin⁷ , Bent Ehresmann⁶ , Daniel Matthiä⁴ , and Bin Zhuang⁸

¹Deep Space Exploration Laboratory, School of Earth and Space Sciences, University of Science and Technology of China, Hefei, PR China, ²CAS Center for Excellence in Comparative Planetology, USTC, Hefei, PR China, ³Institute of Experimental and Applied Physics, Christian-Albrechts-University, Kiel, Germany, ⁴German Aerospace Center (DLR), Institute of Aerospace Medicine, Cologne, Germany, ⁵Space Research and Technology Institute, Bulgarian Academy of Sciences, Sofia, Bulgaria, ⁶Solar System Science and Exploration Division, Southwest Research Institute, Boulder, CO, USA, ⁷Leidos Corporation, Houston, TX, USA, ⁸Institute for the Study of Earth, Oceans, and Space, University of New Hampshire, Durham, NH, USA

Correspondence to:

J. Guo,
jguo@ustc.edu.cn

Citation:

Guo, J., Li, X., Zhang, J., Dobynde, M. I., Wang, Y., Xu, Z., et al. (2023). The first ground level enhancement seen on three planetary surfaces: Earth, Moon, and Mars. *Geophysical Research Letters*, 50, e2023GL103069. <https://doi.org/10.1029/2023GL103069>

Received 31 JAN 2023
Accepted 24 MAR 2023

Abstract On 28 October 2021, solar eruptions caused intense and long-lasting solar energetic particle (SEP) flux enhancements observed by spacecraft located over a wide longitudinal range in the heliosphere. SEPs arriving at Earth caused the 73rd ground level enhancement (GLE) event recorded by ground-based neutron monitors. In particular, this is also the first GLE event seen on the surface of three planetary bodies, Earth, Moon, and Mars, by particle and radiation detectors as shown in this study. We derive the event-integrated proton spectrum from measurements by near-Earth spacecraft and predict the lunar and martian surface radiation levels using particle transport models. Event doses at the lunar and martian surfaces of previous GLE events are also modeled and compared with the current event. This statistical and comparative study advances our understanding of potential radiation risks induced by extreme SEP events for future human explorations of the Moon and Mars.

Plain Language Summary Human beings are considering going back to the Moon and eventually to Mars within the next decades. However, we are still facing one major hurdle “space radiation” which is a significant and unavoidable risk for crews' health, especially for long-term stays at future lunar or martian stations. In particular, sporadic solar energetic particles (SEPs) generated via extreme solar eruptions may enhance the lunar or martian surface radiation levels to potentially hazardous values. Recent lunar and martian surface and orbital radiation detectors have advanced our understanding of the radiation environment of both planetary bodies. On 28 October 2021 a SEP event occurred and had energies high enough to trigger ground-level-enhancement (GLE) events on the surface of Earth, the Moon, and Mars. Combining both measurements and modeling approaches, we study this first GLE event seen on three planetary surfaces and demonstrate its potential SEP radiation risk to humans on the Moon and Mars together with the results of previous GLE events.

1. Introduction

Space radiation induced by solar energetic particles (SEPs), associated with solar eruptions, may potentially expose aerospace activities, satellite industry and human space exploration to significantly increased radiation levels. During historically large SEP events, protons of energies up to a few GeVs may contribute to the Earth's surface particle fluxes and be detected by ground-based neutron monitors (NMs) during so-called ground level enhancement (GLE) events (e.g., Miroshnichenko et al., 2013). From February 1942 to October 2021, 73 GLE events have been registered (<https://gle.oulu.fi/>). The most recent event, namely GLE73, occurred on 28 October 2021 and is the first GLE event of Solar cycle 25. This event is closely associated with an X1.0 class flare and its accompanying strong coronal mass ejection (CME) eruption reaching a speed of >1,300 km/s (Li et al., 2022).

Despite of the long history of GLE events being detected on Earth's surface, multi-point observations of these extreme SEP events at other vantage points within the heliosphere have only become available recently. In particular, particle and radiation detectors are now operating both at the Moon and Mars, on the surface and in orbit, allowing us to study the radiation impact of SEPs, and thereby supporting future lunar and martian missions.

© 2023. The Authors. Geophysical Research Letters published by Wiley Periodicals LLC on behalf of American Geophysical Union.

This is an open access article under the terms of the [Creative Commons Attribution License](https://creativecommons.org/licenses/by/4.0/), which permits use, distribution and reproduction in any medium, provided the original work is properly cited.

As our Moon is in the vicinity of Earth, it is not surprising that during the GLE73 event, both its surface and orbital radiation detectors, which are the lunar Lander Neutron and Dosimetry (LND, Wimmer-Schweingruber et al., 2020) Experiment aboard the Chang'E4 Lander and the Cosmic Ray Telescope for the Effects of Radiation (CRaTER, Spence et al., 2010) in lunar orbit, detected significant enhancements of the lunar radiation level. Additionally, it is intriguing that Mars, separated by 191° longitudinally from Earth, also registered a GLE event on its surface as measured by the Radiation Assessment Detector (RAD, Hassler et al., 2012) on NASA's Curiosity rover. The exact origin of relativistic particles spreading over such a large heliospheric longitude during this and similar events is still under debate, with some suggesting that the particles are accelerated at the CME-driven shock (Papaioannou et al., 2022), while others emphasize the magnetic reconnection and confining process during the eruption (Klein et al., 2022).

In this letter, we focus on the event's radiation impact on the Moon and Mars. We compare and analyze the radiation dose data from Earth, Moon, and Mars (Section 2). We further study the event flux and spectrum (Section 3) which is used to model the lunar and martian surface radiation levels that can be compared to the in-situ measurements (Section 4). We also model the impact of past GLEs on the lunar and martian radiation environment (Section 4) to assess the potential radiation risks induced by extreme SEP events for future human explorations of the Moon and Mars.

2. Radiation Dose Measurements at Earth, Moon, and Mars

First we show the event dose rate measured by various detectors in the vicinity of Earth, Moon, and Mars. Dose rate (in units of J/kg/s or Gray/s) is the radiation energy deposited by incoming particles per unit time to the absorber of unit mass and is often measured in silicon detectors. Sometimes when evaluating the biological effect, dose in silicon is converted into dose in water with a conversion factor of about 1.33 accounting for the comparatively larger ionization potential of silicon. Note that, however, variation of this factor can be expected when accounting for detector size, shape, material, and the varying radiation source (Banjac et al., 2019).

The LND on the backside of the lunar surface consists of a stack of 10 dual-segment (inner and outer segments) silicon solid-state detectors (SSDs), A–J, and the dose rate is measured in the second topmost detector B (Wimmer-Schweingruber et al., 2020; S. Zhang et al., 2020). LND only functions during local lunar daytime and has to be switched off during the cold nighttime. Therefore, its measurements are continuous for about 14 Earth days followed by 14 days of gap time. The GLE73 event is hence only seen during its declining phase by LND, shown in red in Figure 1a, while the event onset and peak (for nearly 2 days) are unfortunately not covered by LND.

Meanwhile, the CRaTER instrument orbiting the Moon captured the entire duration of the event, albeit with lower cadence during the peak time. CRaTER has three pairs of SSDs, namely D12, D34, and D56, separated by the thick tissue equivalent plastic (TEP) which simulates soft body tissue (muscle) shielding of the incoming radiation (Spence et al., 2010). During normal operational mode, D12 points toward deep space, D56 points to the lunar surface while D34 is in the middle. The CRaTER team routinely corrects its data from the orbit to the surface considering that the shielding of primary radiation by the Moon body itself varies with the orbital height and should be 2π on the lunar surface. Note that this assumption may face challenges when the surface albedo radiation from the Moon plays an important role. Figure 1a shows the dose rates measured by the different CRaTER detectors (corrected to the surface) and LND “B” detector. One can see that the dose rates recorded by the different CRaTER detectors agree very well before the SEP onset when background galactic cosmic rays (GCR) were dominating, but they differ significantly throughout most of the event duration with D12 measurement much higher and D34 detecting the lowest values. This is likely because SEPs, in comparison to GCRs, have generally lower energies and are more sensitive to the TEP shielding structure of the instrument. D12 sees more SEPs from deep space and D56 sees lunar albedo particles from the surface and some SEPs from the side (deep space), while D34, being sandwiched in the middle, is shielded against low-energy particles from both sides.

Due to the notable discrepancy, we cannot rely on the CRaTER data “corrected to the surface” to be a measure of the lunar surface radiation during the event. In order to reconstruct the surface radiation level when LND was switched off, we correlate the LND and CRaTER data during the SEP event (marked in the gray shaded area) and find correlations that can further predict the lunar surface dose rate. The procedure is shown in Figures 1b and 1c. The surface radiation predicted by the D34 & LND correlation and the D56 & LND correlation, that is,

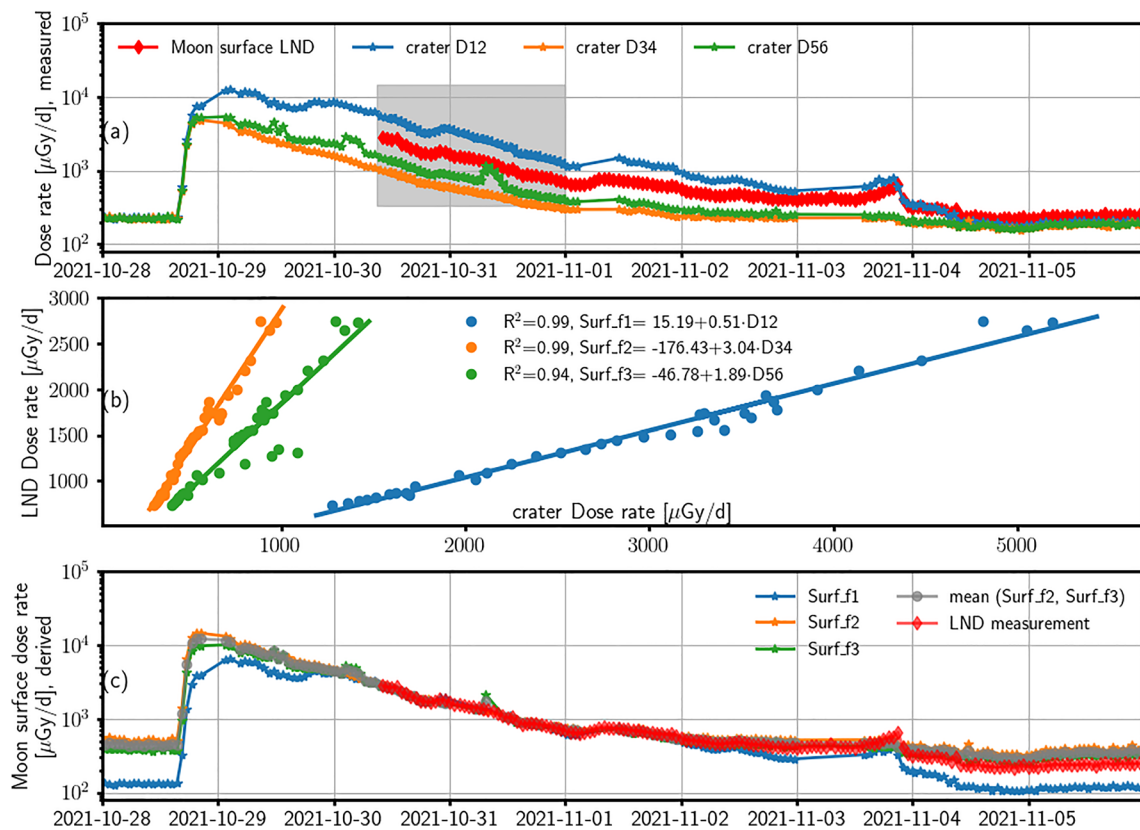


Figure 1. (a) The dose rates measured by different Cosmic Ray Telescope for the Effects of Radiation (CRaTER) detector pairs (corrected to the surface) and the Lander Neutron and Dosimetry (LND) “B” detector. (b) Correlation of the LND data and different CRaTER measurements during the time period marked in the gray area in (a). (c) The surface radiation measured by LND and predicted by different CRaTER-LND correlations derived in (b). More explanations are in the text.

“Surf_f2” and “Surf_f3” in (c), agree very well, while the correlation of D12 & LND in the shaded region results in a relatively poor prediction of “Surf_f1” near the event onset and end resulting in a much lower GCR background and a lower dose rate compared to the actual LND measurement at the declining phase. Therefore, we use the averaged D34 & LND and D56 & LND prediction for time periods when LND data are missing.

Near Earth, there are also various instruments monitoring the radiation environment, mounted either on-board satellites or the International Space Station. Here we use the Radiation Measurement In Space (RAMIS) instrument data onboard the German Eu:CROPIS satellite (Hauslage et al., 2018) circling at an ~600 km polar orbit since December 2018. RAMIS uses a silicon detector telescope with two detectors D1 and D2. Similar to CRaTER in lunar orbit, RAMIS measures the deep space radiation where no planetary shielding is present and Earth’s albedo radiation within the view angle of Earth itself, with the former making a dominant contribution to the top detector D1. Selected data from D1 are collected at high latitude (polar regions) with the vertical geomagnetic cutoff rigidity close to zero, as plotted in green in Figure 2a. It shows a very similar temporal evolution, with slightly smaller values, compared to the lunar surface dose rate (derived values in empty gray circles and LND-measured values in gray dots). This is likely because RAMIS D1 is located behind 3 mm of Aluminum shielding which stops vertical incident protons below about 24 MeV, while LND B detector is only shielded by the 0.5 mm-thick A detector from the top (although the shielding of LND from the side and the bottom by the lander itself is nonuniform and can be much higher). The lunar orbital measurement by CRaTER D12 (now “uncorrected” back to the orbit) is shown in brown as a comparison. As it is the least shielded instrument directly exposed to SEPs coming from deep space which occupies most of the instrumental solid angle, its dose rate is much higher than LND and RAMIS measurements and also shows more significant bumpy structures related to the low-energy component of the SEP flux as later shown in Figure 3.

At Mars’ orbit, the Liulin-MO dosimeter (Semkova et al., 2018) onboard the ExoMars Trace Gas Orbiter (TGO) has been investigating the radiation conditions at a 400-km circular orbit since May 2018. Liulin-MO contains

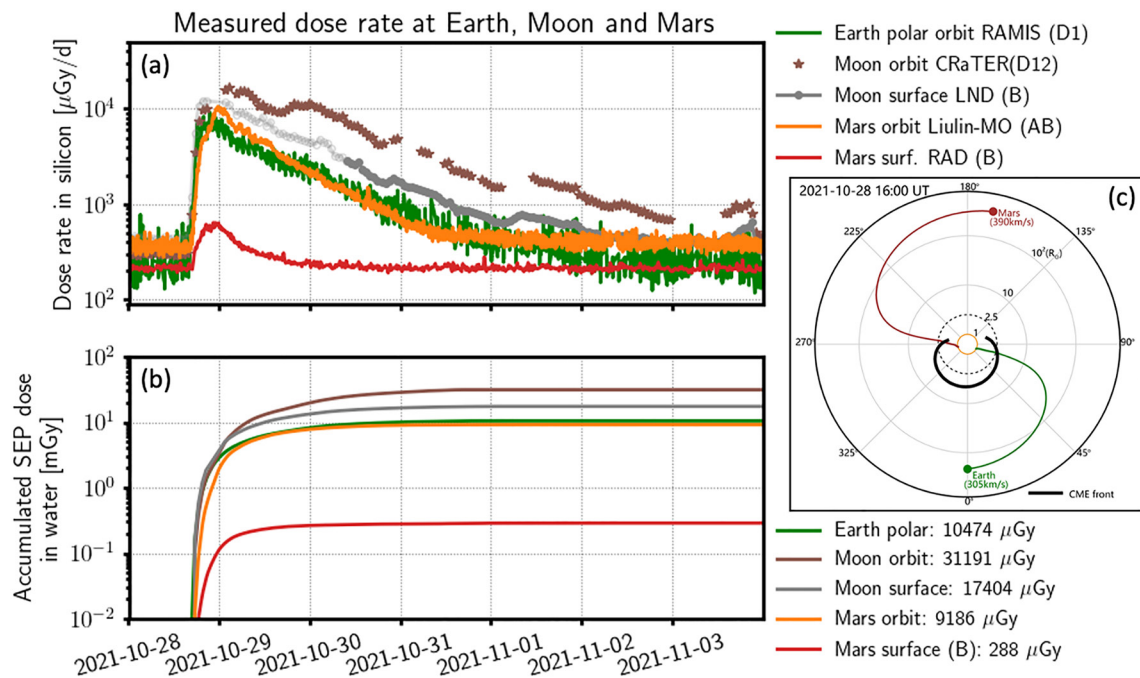


Figure 2. (a), (b) The measured dose rate at Earth's orbit by RADIATION Measurement In Space (D1 detector), at lunar surface by Lander Neutron and Dosimetry (B detector) and orbit by Cosmic Ray Telescope for the Effects of Radiation (D12 detectors), and at martian surface by Radiation Assessment Detector (B detector) and orbit by Liulin-MO (AB detectors). (a) shows the measured dose rate in silicon whilst (b) shows the galactic cosmic rays background subtracted and sporadic solar energetic particle-event accumulated dose (converted to dose in water), with the total event dose shown in the legend. (c) View of the ecliptic plane from solar north in logarithmic radial scale, showing the positions of Earth, Mars, and the coronal mass ejection front on 28 October 2021 at 16:00 UT. The curves connecting Earth/Mars and the solar surface are derived magnetic field lines (more explanations in the main text).

two dosimetric telescopes, AB and CD, arranged at perpendicular directions. During nominal status, the axes of BA and DC are both 90° from the nadir. A and B (or C and D) have different and complementary energy response ranges so that together they measure the dose rate. In Figure 2, we show only the AB dose rate which is less noisy than CD data. The Mars orbit dose rate temporal evolution shows very similar profiles to that at Earth orbit, except for a slight delay of the onset and peak time. This is intriguing considering that the flare/CME was directed toward Earth in longitude (West 0° – 2° and South 26° – 28° as seen from Earth) while Mars was located at the backside of the Sun from the eruption site (Figure 2c).

Detailed analysis considering the CME evolution (Figure 2c and more details in Li et al., 2022) and the in-situ solar wind speed at Earth/Mars shows that both planets could have had a direct magnetic connection to the potential acceleration source (the shock front) which allows for the most efficient particle transport. It is shown that during the early eruptive phase when acceleration was most efficient, Earth and Mars were nearly symmetrically connected to the east and west sides of the shock which may have had similar effectiveness of acceleration assuming lateral-symmetrical expansion of the shock (e.g., Veronig et al., 2018). This could explain why the dose rate profiles at two locations are rather similar. It is also interesting to note that if Mars were much closer to the Sun (the current distance is 1.6 AU), its magnetic footprint connected by a Parker spiral to the Sun should be further away (longitudinally) from the eruption center and it might detect much less SEP radiation enhancement.

On Mars' surface, RAD has been detecting energetic particle radiation as part of the Mars Science Laboratory (MSL) mission which landed the Curiosity rover in Gale crater in August 2012 (Hassler et al., 2014). From top to bottom, RAD consists of three SSDs (A, B and C, each having a thickness of $300 \mu\text{m}$), and two different scintillators D and E. In particular, dose rate is measured concurrently in two active dosimeters, that is, detectors B and E. To ease the comparison with other silicon detectors, we adopt “B” measurement as plotted in red in Figure 2. In comparison with other measurements, the Mars' surface radiation dose is much smaller during the SEP event and only shows an enhancement during the first 1.5 days of the event. This is because with the martian atmospheric shielding, only protons with energy above about 150 MeV can penetrate to the martian surface and contribute to RAD's measurement (Guo et al., 2019). Since these high-energy SEPs are mainly accelerated during the initial

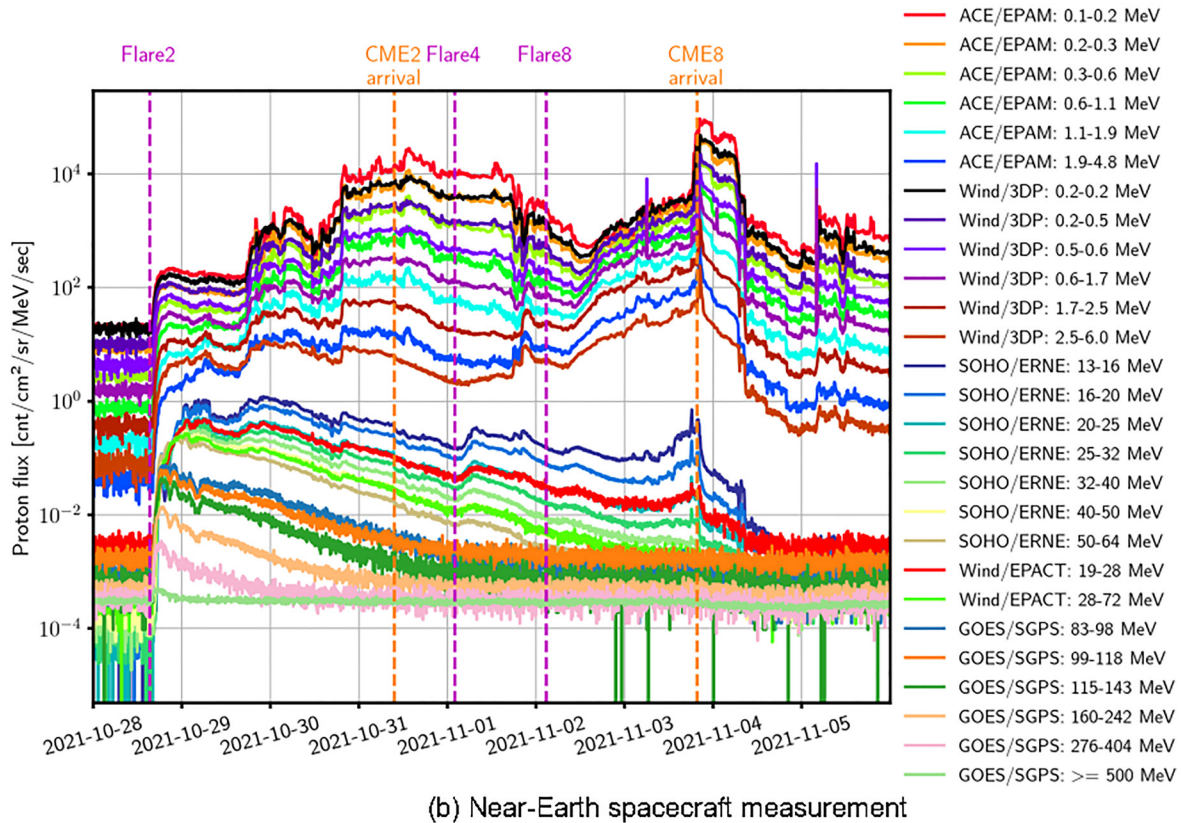
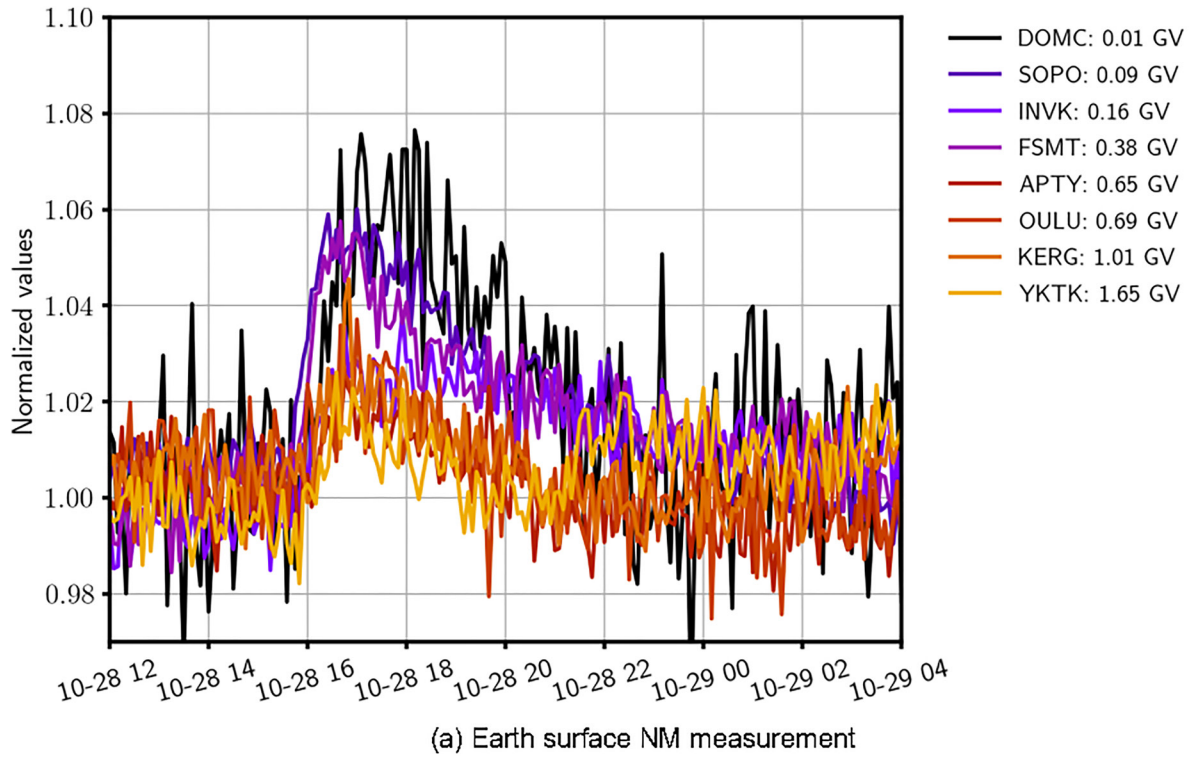


Figure 3. (a) The relative enhancement measured by different neutron monitors with different geomagnetic cutoff rigidities (shown in legend). (b) Proton flux from 28 October to 6 November 2021 detected by Advanced Composition Explorer/Electron and Proton Alpha Monitor (EPAM), Wind/3DP, Solar and Heliospheric Observatory/The Energetic and Relativistic Nuclei and Electron (ERNE) sensor, Wind/The Energetic Particles, Acceleration, Composition and Transport (EPACT) Experiment, and GOES16/Solar and Galactic Proton Sensor (SGPS) detectors at various energy ranges. More details are given in the main text.

eruption phase, they are primarily detected at the early phase of the SEP event (also see high-energy components in Figure 3b).

Figure 2b shows SEP accumulated dose (with the GCR background subtracted and converted to dose in water). Lunar orbit dose is the highest while martian surface dose is the lowest for this event. The radiation reduction from Mars orbit to surface is mostly due to the shielding of the atmosphere as explained earlier. However, it is nontrivial to compare and explain the discrepancies between different orbital measures at 3 locations due to the differences in both planetary shielding and albedo contributions as each orbit scenario corresponds to a different ratio of planetary shielding of the primary radiation and each planet has a different albedo radiation contribution to the orbital measurement. Besides, SEPs may have strong spatial anisotropies which differ at different locations especially during its initial phase (e.g., Dressing et al., 2014) and SEP detection at planet's orbit is constrained by both the direction of the incoming SEPs and the shielding condition around detector.

3. Particle Measurements at Earth

Various Earth-ground NMs have detected the GLE73 event as shown in Figure 3a with 5-min data (from the neutron monitor database, <https://www.nmdb.eu/data/>) normalized to the pre-event background level of each NM. Each station's name and its geomagnetic cutoff rigidity are marked in the legend. It is clearly shown that the relative enhancement is larger for stations with smaller cutoff rigidities which allow more SEPs to enter the Earth's magnetosphere. More detailed analysis of the GLE73 event can be found in Papaioannou et al. (2022) and Mishev et al. (2022).

To reveal the properties of relativistic SEPs associated to GLE events, the identification of the primary SEP spectrum is necessary. We therefore load energy-dependent spacecraft data from particle detectors onboard the Advanced Composition Explorer (ACE, Stone et al., 1998), Wind (Acuña et al., 1995), Solar and Heliospheric Observatory (SOHO, Domingo et al., 1995) and the Geostationary Operational Environmental Satellite (GOES, e.g., Kress et al., 2020) as shown in Figure 3b. Note that the last channel of GOES was originally an integral channel for protons above 500 MeV. Here in order to derive the energy-differential flux, we assume an upper bound of 1.6 GeV for this channel which is the upper energy of this event constrained by ground-based NM detection (Papaioannou et al., 2022). The geometric mean of the bin edges that is 894 MeV is approximated as the effective energy of this channel. Therefore, flux of this channel is more reliable during the SEP event than during the quiet time when the dominating flux is from GCRs which have a much wider energy range.

The temporal profile of proton flux shown in Figure 3b has many complex structures related to solar eruptions and the pass-by of heliospheric disturbances which deserve detailed investigations in another study. Here we include some vertical lines marking the time of a few relevant events analyzed by Li et al. (2022) who used both the remote-sensing and in-situ data throughout this period and found eight pairs of flares and CMEs. We mark the onset times of Flare2 (associated with GLE73) and Flare4 which had a direct magnetic connection to Earth with corresponding SEPs arriving after the events. The identified in-situ arrivals of CME2 and CME8 (orange lines) are followed by enhanced flux of protons with energy below 10 MeV, especially upon CME8's arrival which corresponds to a much stronger in-situ shock (Li et al., 2022). These so-called energetic storm particles (ESPs) are believed to be accelerated by interplanetary shocks as they propagate outward (C. M. Cohen, 2006).

We also note that right after the onset of Flare2, the flux enhancement at proton energies below about 6 MeV (by ACE/Electron and Proton Alpha Monitor and Wind/3DP) is likely a contamination of secondary particles from the interaction of high-energy SEPs with spacecraft and instrument structure. Therefore the fluxes of these channels before 29 October 2021 12:00 UT are excluded from the following spectral analysis.

The event-integrated energy spectrum from 28 October 16:00 UT until Nov 1st 02:00 UT (i.e., between Flare2 and Flare4 in Figure 3b) across different detectors' energies are marked in Figure 4a (red curve) and fitted by a band function (Band et al., 1993) as following:

$$\Phi_{Band}(E) = AE^{-\gamma_a} \exp(-E/E_0), \text{ for } E < (\gamma_b - \gamma_a)E_0 \quad (1)$$

$$= AE^{-\gamma_b} [(\gamma_b - \gamma_a)E_0]^{(\gamma_b - \gamma_a)} \exp(\gamma_a - \gamma_b), \text{ for } E > (\gamma_b - \gamma_a)E_0, \quad (2)$$

where $A = (1.12 \pm 0.44) \times 10^8$ counts/MeV/cm², $E_0 = 101.5 \pm 21.8$ MeV, $\gamma_a = 1.47 \pm 0.13$, $\gamma_b = 3.34 \pm 0.15$.

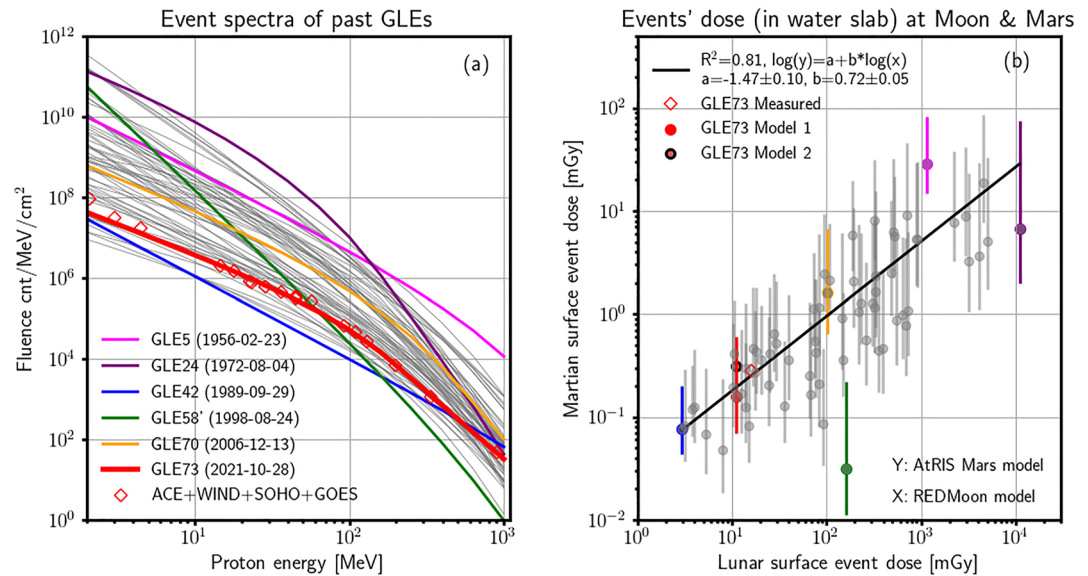


Figure 4. (a): The event-integrated solar energetic particle spectrum of GLE73 derived from spacecraft data fitted by a band function (red), in comparison with previous ground level enhancement (GLE) spectra. (b): The modeled event-integrated dose on martian surface (by AtRIS/Mars model) versus that on lunar surface (by REDMoon model) for each GLE event shown in (a). Each errorbar for the Mars modeling results indicates the upper and lower bounds of the event dose under different surface pressure conditions. A few events are in matching colors with their spectra and GLE dates shown in (a). Note GLE58' corresponds to the energetic storm particle component of the event (Raukunen et al., 2018).

To compare this event spectrum with previous ones, we also plot the event spectra summarized by Raukunen et al. (2018, 65 spectra in Table 2) using spacecraft and ground-based data. Each event spectrum has been fitted by a band function as plotted in Figure 4a which shows that GLE73 has an event-integrated flux relatively low as compared to the previous events, especially at energy below 10s of MeV.

4. Modeling GLE-Induced Radiation Levels on the Moon and Mars

The GLE event spectra shown above can be used to model SEP induced radiation doses at the Moon and Mars. Since Moon and Earth are close neighbors in the heliosphere, it is reasonable to assume that these spectra derived at Earth can be directly applied to the Moon. Alternatively, since SEP flux distribution in the heliosphere is highly variable and may depend on both the radial and longitudinal distances from the flare/CME site (e.g., Lario et al., 2013), it is nontrivial to derive the SEP flux from Earth to Mars with a different heliospheric location. As the relative longitudinal separation of the flare/CME site to either Mars or Earth is arbitrary and thus statistically equivalent for many events, we here scale the flux from Earth to Mars only considering the radial gradient. In a simple spherical coordinate where particles expand outwards from the spherical center, a simple scaling factor of $1/r^2$ can be applied to the particle flux, that is, the event fluence (with unit of counts/MeV/cm²) at Mars ($r \sim 1.5$ AU from the Sun) is about $1/1.5^2$ times of that at Earth (at 1 AU Solar distance).

Since our Moon does not have a global magnetic field or an atmosphere, SEPs can reach the lunar surface directly and also interact with the lunar soil to generate so-called upward "albedo" radiation (e.g., Xu et al., 2022). Mars also lacks a global intrinsic magnetosphere but instead has a thin atmosphere, where SEPs can directly propagate through or lose part of its energy and generate secondaries. When reaching the surface, these particles may also interact with the martian soil to induce the surface albedo radiation (e.g., Guo et al., 2021). The interaction of particles with the lunar or martian environment has been studied via particle transport modeling through the planetary atmosphere and regolith (e.g., Banjac et al., 2018; Kim et al., 2014; Matthiä et al., 2016, 2017; Mesick et al., 2018; Naito et al., 2020). Here, we use the state-of-the-art lunar radiation model "REDMoon" (Dobynde & Guo, 2021) and martian radiation model "AtRIS/Mars" (Guo et al., 2019) to calculate the induced radiation field by these GLE events on the surfaces of the Moon and Mars, respectively.

For each event, first the spectra of different particles (including primary and secondary protons, neutrons, electrons, gammas etc.) in both the upward and downward directions on the planetary surface are obtained. Then they

are assumed to impinge onto a 0.5 mm silicon slab which is chosen to be comparable to aforementioned radiation detectors, while the rest of the specific instrument/spacecraft is not considered. The total event dose in the silicon slab is then converted to dose in water using the silicon-water conversion factor 1.33 to ease the assessment of radiation effects on humans.

The surface pressures on Mars may differ significantly from one location to another resulting in different atmospheric shielding conditions for incoming energetic particles (J. Zhang et al., 2022). Therefore we perform six sets of modeling processes under martian surface pressures of 305, 530, 750, 975, and 1,200 Pa (J. Zhang et al., 2022, Figure 2) to assess the variation of the SEP radiation on different martian locations (or altitudes). We take 750 Pa as the “reference pressure” since it is closest to the pressure (742 Pa) during the GLE73 event observed by MSL in Gale crater. The modeled result of each event is shown in Figure 4b with the x and y axes for lunar and martian surface doses, respectively. The dot itself in y corresponds to the reference pressure result. The errorbar gives the minimum and maximum doses of the event on Mars which normally result from maximum pressure (1,200 Pa) and minimum pressure (305 Pa), respectively. The correlation between the GLE-induced martian surface dose and lunar surface dose in log scale has been obtained as: $D_{Mars} = C \cdot D_{Moon}^b$, where $C = (3.4 \pm 0.8) \times 10^{-2}$ and $b = 0.72 \pm 0.05$ with the Pearson correlation $R^2 = 0.81$.

The results of a few events are shown in matching colors in Figures 4a and 4b, including the ones causing the maximum and minimum doses on the Moon (GLE24 and GLE42), the ones causing the maximum and minimum doses on Mars (GLE5 and GLE58’s ESP component), as well as GLE70 and GLE73. Comparing the spectral shape and their doses, we notice that SEP fluxes between about 10 and 100 MeV dominate the lunar surface dose while fluxes above about 200 MeV dominate the martian surface dose. The same event may also result in completely different surface doses on different locations on Mars (up to about a factor of 35). This highlights the importance of understanding both the SEP spectral properties and the planetary environment for predicting their radiation impacts on the surface of Moon/Mars.

The modeled and measured GLE73 doses are slightly different. For lunar surface, the modeled event dose is about 11 mGy while the measurement reaches about 17 mGy. But it is difficult to explain this since the lunar surface data during the first 2 days of the event were derived using CRaTER data and this procedure carries unknown uncertainties. On the other hand, the Mars surface measurement is 0.288 mGy in RAD “B” (converted to water) while the modeled dose under 750 Pa is 0.159 mGy (“GLE73 Model1” in Figure 4b). This is likely because that the general $1/r^2$ scaling of the SEP fluence is not accurate for this particular event. As already shown by the comparable doses measured at Earth and Mars orbit, if we rescale the SEP flux by the dose ratio (9186/10474, Figure 2) instead of $1/r^2$, we predict the martian surface dose to be 0.315 mGy (“GLE73 Model2” in Figure 4b), a value much more comparable to the measured 0.288 mGy.

5. Summary and Conclusion

We analyzed the first GLE event detected at three planetary bodies: Earth, Moon, and Mars with a focus on the radiation dose rate measurement. We derived the event-integrated SEP spectra at Earth and used particle transport models to calculate the lunar and martian surface radiation levels which are compared with measurements. The modeling approach is also applied to previous GLEs and a statistical correlation between the lunar and martian surface radiation dose is derived. We also showed the significant atmospheric shielding effect on SEPs so that higher altitudes on Mars (with lower pressures) can have much higher event doses.

Both the event-spectrum and the radiation impact of the GLE73 are modest compared to previous GLEs, which may be due to the fact that (a) the parent CME/flare acceleration is not as efficient as for other events with higher total doses, and/or (b) the magnetic connectivity between the observer and the SEP source region is suboptimal (e.g., C. M. S. Cohen et al., 2021, and references therein). More multi-spacecraft observations of extreme types of SEPs would be helpful to better understand and predict the spatial distribution of the radiation environment in the inner-heliosphere during the event.

Our results suggest that for future astronauts going to the Moon or Mars, extreme SEP events (GLE-type) can induce significant radiation risks. Specifically, Acute Radiation Syndrome (ARS, <https://www.cdc.gov/nceh/radiation/emergencies/arsphysicianfactsheet.htm>) can occur when large amount of dose, above ~ 700 mGy, is delivered to the entire body within a short period of time. None of the events on Mars have passed this threshold, but 12 out of the total 67 events over the course of 66 years (on average one event every 5.5 years) have exceeded

this level on the Moon. However, more detailed modeling including shielding around astronauts by a spacesuit shield or even a habitat and also human body geometries should be considered for an accurate quantification of the radiation impact on future Lunar explorers.

Data Availability Statement

We acknowledge the following data sources: CRaTER (<https://crater-web.sr.unh.edu/products.php>), LND (applying via online forms at China National Space Administration, <https://moon.bao.ac.cn/web/zhmanager/noticelist?-detailId=906336> and from the University of Kiel, <https://www.ieap.uni-kiel.de/et/change4/>), TGO/Liulin-MO (<http://esa-pro.space.bas.bg/datasources>), MSL/RAD from NASA planetary data systems (<https://doi.org/10.17189/1519761>), NMDB (<https://www.nmdb.eu/nest/>), GOES (<https://data.ngdc.noaa.gov/platforms/solar-space-observing-satellites/goes/>) and the NASA SPDF (https://spdf.gsfc.nasa.gov/data_orbits.html) for other spacecraft data. Data plotted in the figures are archived at Zenodo <https://doi.org/10.5281/zenodo.7741220>.

References

- Acuña, M., Ogilvie, K., Baker, D., Curtis, S., Fairfield, D., & Mish, W. (1995). The global geospace science program and its investigations. *Space Science Reviews*, 71(1), 5–21. <https://doi.org/10.1007/BF00751323>
- Band, D., Matteson, J., Ford, L., Schaefer, B., Palmer, D., Teegarden, B., et al. (1993). BATSE observations of gamma-ray burst spectra. I-Spectral diversity. *The Astrophysical Journal*, 413, 281–292. <https://doi.org/10.1086/172995>
- Banjac, S., Berger, L., Burmeister, S., Guo, J., Heber, B., Herbst, K., & Wimmer-Schweingruber, R. (2019). Galactic cosmic ray induced absorbed dose rate in deep space—accounting for detector size, shape, material, as well as for the solar modulation. *Journal of Space Weather and Space Climate*, 9, A14. <https://doi.org/10.1051/swsc/2019014>
- Banjac, S., Herbst, K., & Heber, B. (2018). The atmospheric radiation interaction simulator (AtRIS)—Description and validation. *Journal of Geophysical Research: Space Physics*, 123(ja), 50–67. <https://doi.org/10.1029/2018JA026042>
- Cohen, C. M. (2006). Observations of energetic storm particles: An overview. *Geophysical Monograph—American Geophysical Union*, 165, 275. <https://doi.org/10.1029/165GM26>
- Cohen, C. M. S., Li, G., Mason, G. M., Shih, A. Y., & Wang, L. (2021). Solar energetic particles. In N. E. Raouafi & A. Vourlidis (Eds.), *Solar physics and solar wind* (Vol. 1, p. 133). <https://doi.org/10.1002/9781119815600.ch4>
- Dobynde, M. I., & Guo, J. (2021). Radiation environment at the surface and subsurface of the Moon: Model development and validation. *Journal of Geophysical Research: Planets*, 126(11), e2021JE006930. <https://doi.org/10.1029/2021JE006930>
- Domingo, V., Fleck, B., & Poland, A. (1995). SOHO: The solar and heliospheric observatory. *Space Science Reviews*, 72(1), 81–84. <https://doi.org/10.1007/BF00768758>
- Dresing, N., Gómez-Herrero, R., Heber, B., Klassen, A., Malandraki, O., Dröge, W., & Kartavykh, Y. (2014). Statistical survey of widely spread out solar electron events observed with STEREO and ACE with special attention to anisotropies. *Astronomy & Astrophysics*, 567, A27. <https://doi.org/10.1051/0004-6361/201423789>
- Guo, J., Banjac, S., Röstel, L., Terasa, J. C., Herbst, K., Heber, B., & Wimmer-Schweingruber, R. F. (2019). Implementation and validation of the GEANT4/AtRIS code to model the radiation environment at Mars. *Journal of Space Weather and Space Climate*, 9(A2), A7. <https://doi.org/10.1051/swsc/2019004>
- Guo, J., Khaksarighiri, S., Wimmer-Schweingruber, R. F., Hassler, D. M., Ehresmann, B., Zeitlin, C., et al. (2021). Directionality of the Martian surface radiation and derivation of the upward albedo radiation. *Geophysical Research Letters*, 48(15), e2021GL093912. <https://doi.org/10.1029/2021GL093912>
- Hassler, D. M., Zeitlin, C., Wimmer-Schweingruber, R. F., Böttcher, S. I., Martin, C., Andrews, J., et al. (2012). The Radiation Assessment Detector (RAD) investigation. *Space Science Reviews*, 170(1), 503–558. <https://doi.org/10.1007/s11214-012-9913-1>
- Hassler, D. M., Zeitlin, C., Wimmer-Schweingruber, R. F., Ehresmann, B., Rafkin, S., Eigenbrode, J. L., et al. (2014). Mars's surface radiation environment measured with the Mars Science Laboratory's curiosity rover. *Science*, 343(6169), 1244797. <https://doi.org/10.1126/science.1244797>
- Hauslage, J., Strauch, S. M., Eßmann, O., Haag, F. W., Richter, P., Krüger, J., et al. (2018). Eu:CROPIS—“Euglena gracilis: Combined regenerative organic-food production in space”—A space experiment testing biological life support systems under lunar and martian gravity. *Microgravity Science and Technology*, 30(6), 933–942. <https://doi.org/10.1007/s12217-018-9654-1>
- Kim, M.-H. Y., Cucinotta, F. A., Nounu, H. N., Zeitlin, C., Hassler, D. M., Rafkin, S. C. R., et al. (2014). Comparison of Martian surface ionizing radiation measurements from MSL-RAD with Badhwar-O’Neill 2011/HZETRN model calculations. *Journal of Geophysical Research: Planets*, 119(6), 1311–1321. <https://doi.org/10.1002/2013JE004549>
- Klein, K.-L., Musset, S., Vilmer, N., Briand, C., Krucker, S., Battaglia, A. F., et al. (2022). The relativistic solar particle event on 28 October 2021: Evidence of particle acceleration within and escape from the solar corona. *Astronomy & Astrophysics*, 663, A173. <https://doi.org/10.1051/0004-6361/202243903>
- Kress, B. T., Rodriguez, J. V., & Onsager, T. G. (2020). Chapter 20—The GOES-R space environment in situ suite (SEISS): Measurement of energetic particles in geospace. In S. J. Goodman, T. J. Schmit, J. Daniels, & R. J. Redmon (Eds.), *The GOES-R series* (pp. 243–250). Elsevier. <https://doi.org/10.1016/B978-0-12-814327-8.00020-2>
- Lario, D., Aran, A., Gómez-Herrero, R., Dresing, N., Heber, B., Ho, G., et al. (2013). Longitudinal and radial dependence of solar energetic particle peak intensities: STEREO, ACE, SOHO, GOES, and MESSENGER observations. *The Astrophysical Journal*, 767(1), 41. <https://doi.org/10.1088/0004-637X/767/1/41>
- Li, X., Wang, Y., Guo, J., & Lyu, S. (2022). Solar energetic particles produced during two fast coronal mass ejections. *The Astrophysical Journal Letters*, 928(1), L6. <https://doi.org/10.3847/2041-8213/ac5b72>
- Matthäi, D., Ehresmann, B., Lohf, H., Köhler, J., Zeitlin, C., Appel, J., et al. (2016). The Martian surface radiation environment—a comparison of models and MSL/RAD measurements. *Journal of Space Weather and Space Climate*, 6(27), 1–17. <https://doi.org/10.1051/swsc/2016008>

Acknowledgments

We acknowledge the Strategic Priority Program of the Chinese Academy of Sciences (XDB41000000), the National Natural Science Foundation of China (42074222, 42188101, 42130204) and the CNSA pre-research Project on Civil Aerospace Technologies (D020104). JS is supported by the government of Bulgaria through an ESA Contract under PECS (4000133961/21/NL/SC). RAD is supported by NASA (HEOMD) under JPL subcontract 1273039 to SWRI, and in Germany by DLR (50QM0501, 50QM1201, and 50QM1701) to the CAU Kiel. LND is supported by DLR (50 JR 1604) to the Christian-Albrechts-University CAU Kiel and the Beijing Municipal Science and Technology Commission (Z181100002918003) and NSFC (41941001).

- Matthiä, D., Hassler, D. M., de Wet, W., Ehresmann, B., Firan, A., Flores-McLaughlin, J., et al. (2017). The radiation environment on the surface of Mars—Summary of model calculations and comparison to RAD data. *Life Sciences in Space Research*, *14*, 18–28. <https://doi.org/10.1016/j.lssr.2017.06.003>
- Mesick, K. E., Feldman, W. C., Coupland, D. D. S., & Stonehill, L. C. (2018). Benchmarking Geant4 for simulating galactic cosmic ray interactions within planetary bodies. *Earth and Space Science*, *5*(7), 324–338. <https://doi.org/10.1029/2018EA000400>
- Miroshnichenko, L., Vashenyuk, E., & Pérez-Peraza, J. (2013). Solar cosmic rays: 70 years of ground-based observations. *Geomagnetism and Aeronomy*, *53*(5), 541–560. <https://doi.org/10.1134/S0016793213050125>
- Mishev, A. L., Kocharov, L. G., Koldobskiy, S. A., Larsen, N., Riihonen, E., Vainio, R., & Usoskin, I. G. (2022). High-resolution spectral and anisotropy characteristics of solar protons during the GLE N°73 on 28 October 2021 derived with neutron-monitor data analysis. *Solar Physics*, *297*(7), 1–23. <https://doi.org/10.1007/s11207-022-02026-0>
- Naito, M., Hasebe, N., Shikishima, M., Amano, Y., Haruyama, J., Matias-Lopes, J. A., et al. (2020). Radiation dose and its protection in the Moon from galactic cosmic rays and solar energetic particles: At the lunar surface and in a lava tube. *Journal of Radiological Protection*, *40*(4), 947–961. <https://doi.org/10.1088/1361-6498/abb120>
- Papaioannou, A., Kouloumvakos, A., Mishev, A., Vainio, R., Usoskin, I., Herbst, K., et al. (2022). The first ground-level enhancement of solar cycle 25 on 28 October 2021. *Astronomy & Astrophysics*, *660*, L5. <https://doi.org/10.1051/0004-6361/202142855>
- Raukunen, O., Vainio, R., Tylka, A. J., Dietrich, W. F., Jiggins, P., Heynderickx, D., et al. (2018). Two solar proton fluence models based on ground level enhancement observations. *Journal of Space Weather and Space Climate*, *8*, A04. <https://doi.org/10.1051/swsc/2017031>
- Semkova, J., Koleva, R., Benghin, V., Dachev, T., Matviichuk, Y., Tomov, B., et al. (2018). Charged particles radiation measurements with Liulin-MO dosimeter of FRENDS instrument aboard ExoMars Trace Gas Orbiter during the transit and in high elliptic Mars orbit. *Icarus*, *303*, 53–66. <https://doi.org/10.1016/j.icarus.2017.12.034>
- Spence, H. E., Case, A., Golightly, M., Heine, T., Larsen, B., Blake, J., et al. (2010). CRaTER: The cosmic ray telescope for the effects of radiation experiment on the lunar reconnaissance orbiter mission. *Space science reviews*, *150*(1–4), 243–284. <https://doi.org/10.1007/s11214-009-9584-8>
- Stone, E., Frandsen, A., Mewaldt, R., Christian, E., Margolies, D., Ormes, J., & Snow, F. (1998). The advanced composition explorer. *Space Science Reviews*, *86*(1), 1–22. <https://doi.org/10.1023/A:1005082526237>
- Veronig, A. M., Podladchikova, T., Dissauer, K., Temmer, M., Seaton, D. B., Long, D., et al. (2018). Genesis and impulsive evolution of the 2017 September 10 coronal mass ejection. *The Astrophysical Journal*, *868*(2), 107. <https://doi.org/10.3847/1538-4357/aaeac5>
- Wimmer-Schweingruber, R. F., Yu, J., Böttcher, S. I., Zhang, S., Burmeister, S., Lohf, H., et al. (2020). The lunar Lander neutron and dosimetry (LND) experiment on Chang'E 4. *Space Science Reviews*, *216*(6), 1–40. <https://doi.org/10.1007/s11214-020-00725-3>
- Xu, Z., Guo, J., Wimmer-Schweingruber, R., Dobynde, M., Kühl, P., Khaksarighiri, S., & Zhang, S. (2022). Primary and albedo protons detected by the Lunar Lander Neutron and Dosimetry experiment on the lunar farside. *Frontiers in Astronomy and Space Sciences*, *9*. <https://doi.org/10.3389/fspas.2022.974946>
- Zhang, J., Guo, J., Dobynde, M. I., Wang, Y., & Wimmer-Schweingruber, R. F. (2022). From the top of Martian Olympus to deep craters and beneath: Mars radiation environment under different atmospheric and regolith depths. *Journal of Geophysical Research: Planets*, *127*(3), e2021JE007157. <https://doi.org/10.1029/2021JE007157>
- Zhang, S., Wimmer-Schweingruber, R. F., Yu, J., Wang, C., Fu, Q., Zou, Y., et al. (2020). First measurements of the radiation dose on the lunar surface. *Science Advances*, *6*(39), eaaz1334. <https://doi.org/10.1126/sciadv.aaz1334>